ACS Macro Letters

Letter

Cite This: ACS Macro Lett. 2019, 8, 1365−1371

pubs.acs.org/macroletters

Multivalent Polymer−Peptide Conjugates: A General Platform for Inhibiting Amyloid Beta Peptide Aggregation

Xing Jiang,[†,‡] Abigail J. Halmes,[†,‡,§] Giuseppe Licari,[‡] John W. Smith,[∥] Yang Song,[‡,§] Edwin G. Moore,[§] Qian Chen,[*,‡,§,∥] Emad Tajkhorshid,[*,‡,§,⊥] Chad M. Rienstra,[*,§,⊥] and Jeffrey S. Moore[*,‡,§,∥]

[‡]Beckman Institute for Advanced Science and Technology, [§]Department of Chemistry, [∥]Department of Materials Science and Engineering, and [⊥]Department of Biochemistry, University of Illinois at Urbana−Champaign, Urbana, Illinois 61801, United States

Supporting Information

ABSTRACT: Protein aggregation is implicated in multiple deposition diseases including Alzheimer's Disease, which features the formation of toxic aggregates of amyloid beta (Aβ) peptides. Many inhibitors have been developed to impede or reverse Aβ aggregation. Multivalent inhibitors, however, have been largely overlooked despite the promise of high inhibition efficiency endowed by the multivalent nature of Aβ aggregates. In this work, we report the success of multivalent polymer−peptide conjugates (mPPCs) as a general class of inhibitors of the aggregation of Aβ_{40}. Significantly delayed onset of fibril formation was realized using mPPCs prepared with three peptide/peptoid ligands covering a range of polymer molecular weights (MWs) and ligand loadings. Dose dependence studies showed that the nature of the ligands is a key factor in mPPC inhibition potency. The negatively charged ligand LPFFD leads to more efficient mPPCs compared to mPPCs with the neutral ligands, and is most effective at 7% ligand loading across different MWs. Molecular dynamics simulations along with dynamic light scattering experiments suggest that mPPCs form globular structures in solution due to ligand−ligand interactions. Such interactions are key to the spatial proximity of ligands and thus to the multivalency effect of mPPC inhibition. Excess ligand−ligand interactions, however, reduce the accessibility of mPPC ligands to Aβ peptides, and impair the overall inhibition potency.

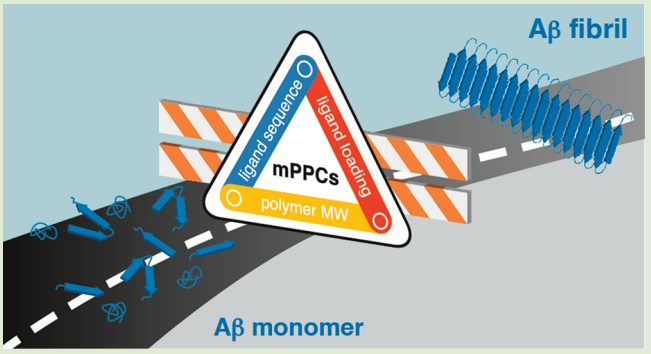

A group of more than 30 different deposition diseases are known to be associated with protein aggregation. For instance, the supramolecular polymerization of amyloid beta (Aβ) peptide[1] and α-synuclein are implicated in Alzheimer's disease (AD) and Parkinson's disease, respectively. In the case of AD, many inhibitors based on peptides and peptidomimetics have been developed to impede Aβ aggregation and alter disease progression.[2,3] The therapeutic outcomes of such efforts have had limited success, due to the inherent challenges of specifically targeting the templated growth of unique Aβ fibril polymorphs and the large surface area of the self-recognition motifs. In this work, we demonstrate that multivalent polymer−peptide conjugation is a general strategy for developing macromolecular Aβ inhibitors[4,5] with enhanced inhibition potency, which depends on the peptide/peptoid ligand sequence, ligand loading percentage, and polymer molecular weight (MW) of the multivalent polymer−peptide conjugates (mPPCs). We previously achieved such multivalency[6,7] by conjugating copies of LPFFD (LD)[8,9] to a flexible poly(*N*-(2-hydroxypropyl)methacrylamide) (PHPMA) backbone.[10,11,12] We demonstrated that LD-mPPCs effectively block Aβ_{40} fibril formation as they redirected Aβ_{40} aggregation from fibrils (Figure 1D, left panels) to small amorphous aggregates (Figure 1D, right panels), as illustrated by TEM and AFM images of representative samples. With the same polymer backbone, mPPCs with 7% LD loading were better inhibitors than those with 3% or 12% loading.[10] We further reported that mPPCs at a constant 7% LD loading disassemble mature fibrils with a dependence on polymer MW.[11,12] However, it remains unclear (1) if the conjugation strategy is applicable to ligands other than LD; (2) how the ligand loading and polymer MW affect mPPC inhibition potency in tandem; and (3) what the origin of such dependence is at the molecular level. Here we report the preparation and inhibition properties of mPPCs of three different ligands, with systematic investigation of ligand loading and polymer MW. MD simulations were performed to better understand the solution conformation, as well as the inhibition dose dependence of mPPCs with different compositions.

Our efforts to thoroughly examine the general chemical space of mPPCs are shown in Figure 1. Central to this study is an examination of the ligand scope of mPPCs. We initially

Received: July 23, 2019
Accepted: September 24, 2019

DOI: 10.1021/acsmacrolett.9b00559
ACS Macro Lett. 2019, 8, 1365−1371

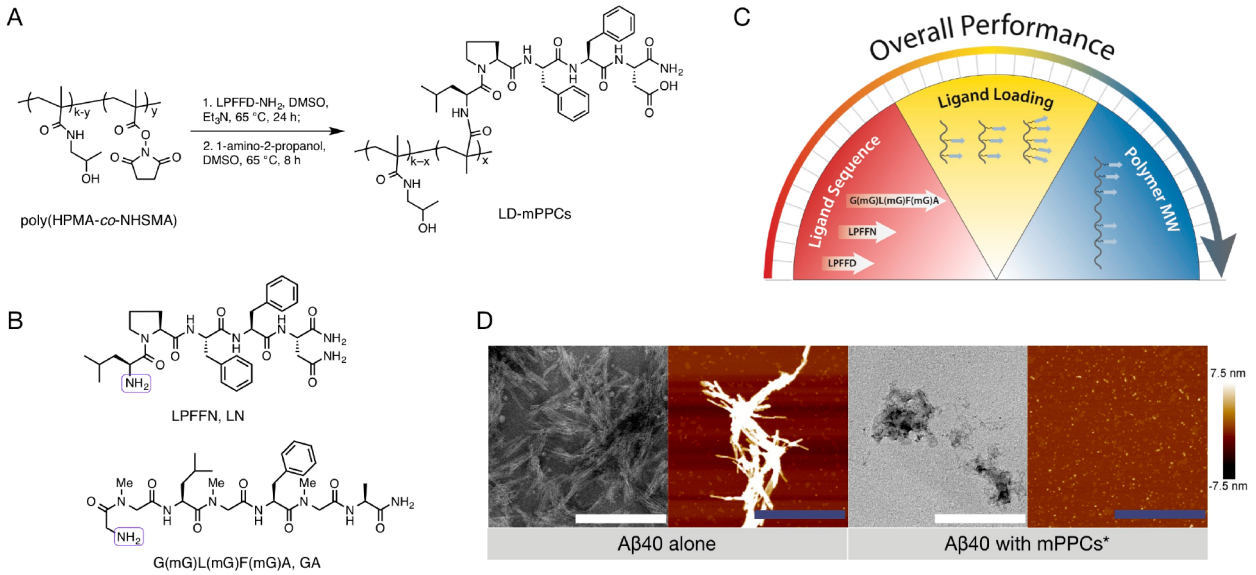

Figure 1. General design of mPPCs for inhibiting Aβ_{40} aggregation. (A) mPPCs are synthesized by the modification of a poly(HPMA-*co*-NHSMA) backbone with an inhibitor ligand, for example, LPFFD (LD). (B) The chemical structures of ligands LPFFN and G(mG)L(mG)F(mG)A with the N-terminal amines used in the polymer−peptide conjugation highlighted. (C) Three independent parameters, the peptide/peptoid ligands, the ligand loading, and the polymer MW are explored in this work for optimizing the inhibition of Aβ aggregation. (D) TEM and AFM images show Aβ_{40} aggregation leading to fibril formation when incubated alone (left panels), but yielding aggregates of a few nanometers in the presence of an mPPC (right panels, see Figure 2B for details). Scale bar: 500 nm.

explored the possibility of using native Aβ sequences including LVFFA, LVFFA-NH_2, KLVFFA-NH_2, KLVFFAE-NH_2, and AIIGL as ligands but failed to obtain any effective conjugates. Peptides LVFFA-NH_2, KLVFFA-NH_2, and KLVFFAE-NH_2 resulted in mPPCs of limited solubility, while the more soluble mPPCs derived from LVFFA and AIIGL were ineffective.[13] We reasoned that ligands from the native sequence inevitably feature strong self-recognition if they are able to interfere with Aβ aggregation, thus, a balance between solubility and inhibition potency is difficult to achieve. We thus focused on other ligands that mimic native Aβ structures while endowing sufficient solubility as they disrupt long-range β-sheet structures. Our previous reports established LD as a prototypical ligand for mPPCs. Here we altered the ligand in two specific ways to investigate the effect of ligand charge and backbone structure, using LPFFN-NH_2 (LN)[14] and G(mG)-L(mG)F(mG)A-NH_2 (GA) as ligands. All three are adapted from the native sequence KLVFFA.[15] We expected LN-mPPCs to be different from LD-mPPCs because of the absence of charge in LN. Peptoid GA, adopted from a known inhibitor thymine-G(mG)L(mG)F(mG)A-NH_2,[16] lacks the key Pro residue in LD and LN, but features *N*-methylation at alternative positions to block the extension of β-sheet structures. The hydrogen bonding behavior between mPPCs and Aβ peptide is distinctive as a result.

With the three ligands identified, a total of 27 mPPCs were prepared by coupling ligand N-terminal amines to the *N*-hydroxysuccinimide (NHS) activated esters on the polymer precursor following literature procedures (see Figure 3C for a complete list of mPPCs, and page S4−S8 of the SI for detailed synthetic procedures).[17,18] Three batches of poly(HPMA-*co*-NHSMA) polymer precursors were used with MW of 18, 43, and 77 kDa (DP = 115, 275, and 493), and a range of ligand loading was explored for each ligand−MW combination. The MWs and loading percentages were chosen based on previous results.[10,11,19] We aimed to prepare LD- and LN-mPPCs of 3−12% loading to test whether 7% loading is optimal for LD-mPPCs of all MWs[10] and how such dependence varies for mPPCs bearing a neutral ligand LN. A higher ligand loading (7−15%) for GA-mPPCs was targeted since GA was reported to be ineffective without a strongly hydrogen-bonding thymine moiety at the N-terminus.[16] All of the 27 mPPCs featured relatively good solubility. Slightly lower loading was achieved for the mPPCs prepared from the 77 kDa precursor, likely due to the increased steric hindrance.

DLS experiments were performed to understand the solution behavior of mPPCs. No aggregation was observed for mPPCs up to 1 mg/mL in PBS buffer, as the hydrodynamic size remained constant after a 25-fold dilution. The diameter of most of the mPPCs is in the range of 4−11 nm (Figure 3C), while the diameter of control PHPMA polymers without ligands (prepared from aminolysis of precursors of 18, 43, and 77 kDa) are 5.7, 7.2, and 8.0 nm, respectively. However, we noticed that two LN-mPPCs of higher MW and ligand loading were much larger than the typical size. We reason that cross-linking occurred due to the harsh conditions required to obtain mPPCs with high loading of LN for high MW polymers.

Thioflavin T (ThT) assays[20] confirmed the importance of polymer−peptide conjugation, as all 27 mPPCs outperformed isolated ligands, isolated PHPMA, and their physical mixtures, with effective inhibition of Aβ_{40} fibril formation at 200 μg/mL (the control experiment data is summarized in Table S3). In the ThT assay, a rapid increase in fluorescence was observed after a certain time when Aβ_{40} (10 μM, 43 μg/mL) was incubated without any inhibitors at 37 °C with shaking (Figure 2A). The interval preceding the sharp increase, known as the lag time, correlates to the Aβ nucleation process in a nucleation−elongation mechanism.[21] At 200 μg/mL, all mPPCs significantly increased the lag time, and in most cases, no onset of fibril formation was observed during the 24 h incubation time. ThT assay results of three representative mPPCs of different ligands, ligand loading, and polymer MW,

DOI: 10.1021/acsmacrolett.9b00559
ACS Macro Lett. 2019, 8, 1365−1371

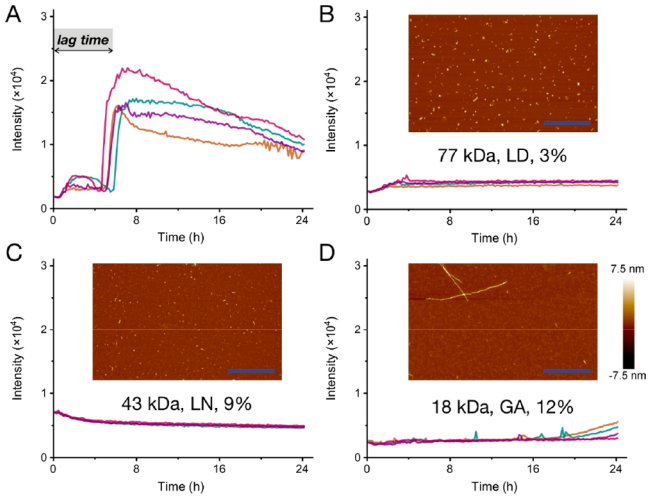

Figure 2. General efficacy of mPPC inhibitors. (A) When incubated alone at 10 μM, Aβ_{40} quickly formed fibrils as detected by an increase of fluorescence intensity in ThT assays. Most mPPCs led to evident inhibition with no fluorescence increase within 24 h at 200 μg/mL, as is shown for (B) LD-mPPC of 77 kDa at 3% loading and (C) LN-mPPC of 43 kDa at 9% loading. (D) GA-mPPC of 18 kDa at 12% loading allowed partial fibril formation with a lag time approaching 24 h. The colored traces represent results from multiple replicas (n = 4). AFM (insets, B–D) confirmed the absence of fibrils for most of the tested mPPCs except for the GA-mPPC. Scale bar: 500 nm.

together with AFM images of the corresponding samples, are shown in Figure 2B–D. Of the three examples, two mPPCs (3% LD, 77 kDa polymer; 9% LN, 43 kDa polymer) completely stopped fibril formation (for simplicity, a lag time of 24 h is assigned to complete inhibition). Only small particles of a few nanometers were observed with AFM (Figure 2B,C). The GA-mPPCs of 18 kDa polymer at 12% loading extended the lag time to approximately 24 h, resulting in a small amount of fibril together with small nanoparticles (Figure 2D).

To compare the relative potency of different mPPCs and to provide guidance for future mPPC design, we studied the dose dependence of their inhibition at a range of concentrations (10, 20, 50, 100, and 200 μg/mL). The experimental data and their analyses are shown in Figure 3A,B for a representative example (9% LN, 43 kDa polymer) of the 27 mPPCs. While this conjugate was capable of completely inhibiting Aβ_{40} fibril formation at 100 and 200 μg/mL during the 24 h incubation, little change was observed compared to the control (Figure 2A) when the concentration was equal to or less than 50 μg/mL. This behavior suggests that a threshold concentration must be reached for mPPCs to be effective. Such an "all or nothing" dose threshold has not been observed for any other inhibitors to the best of our knowledge[22−25] and is inferred to result from the multivalent ligand architecture[26−28] on linear polymer scaffolds.[29−31] To compare the minimum effective concentration for each mPPC, we plotted the relative lag time

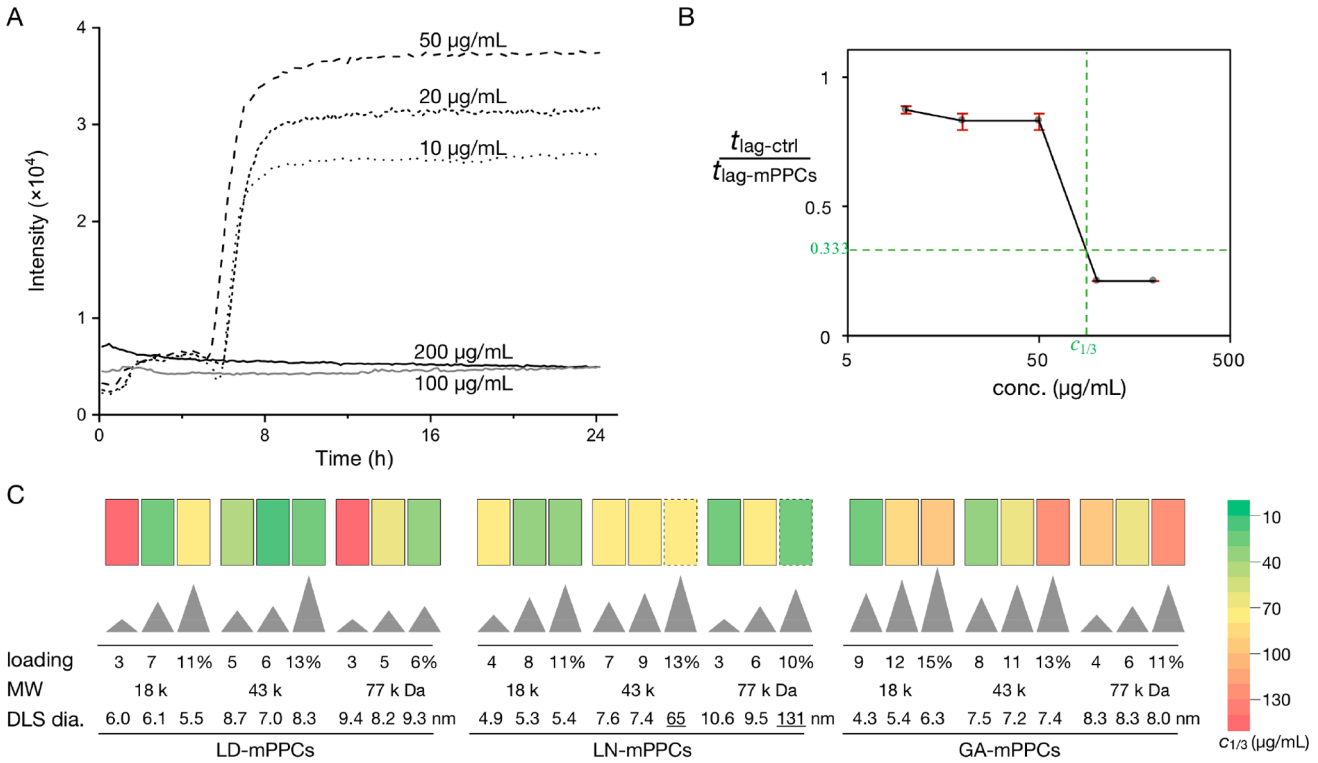

Figure 3. Dose dependence of mPPC inhibition and the evaluation of inhibitory potency of all mPPCs. (A) ThT assays of 10 μM Aβ_{40} in the presence of 10–200 μg/mL LN-mPPCs from 43 kDa polymer with 9% loading. Only one representative trace of four independent measurements at each concentration is shown for clarity. (B) The ratios of the lag time of the control (Aβ alone) to those in the presence of LN-mPPCs are plotted as a function of mPPC concentration. Error bars represent the standard deviation (n = 4). Critical concentration, $c_{1/3}$, defined as the concentration at which mPPCs extend the lag time to 3× that of the control, is obtained directly from the plot. Plots summarizing this analysis for all mPPCs in both mass concentration (mPPCs) and molar concentration (peptide/peptoid ligand) are shown in Figures S2 and S3, respectively. (C) The relative potency of all mPPCs with the color of each bar representing the $c_{1/3}$ value of each mPPC (potency is inversely related to the $c_{1/3}$ value). The height of the gray triangles represents the corresponding ligand loading. The hydrodynamic size of mPPCs is determined by DLS, and the two highlighted LN-mPPCs feature diameters ca. 10× larger than those of their analogs.

DOI: 10.1021/acsmacrolett.9b00559
ACS Macro Lett. 2019, 8, 1365−1371

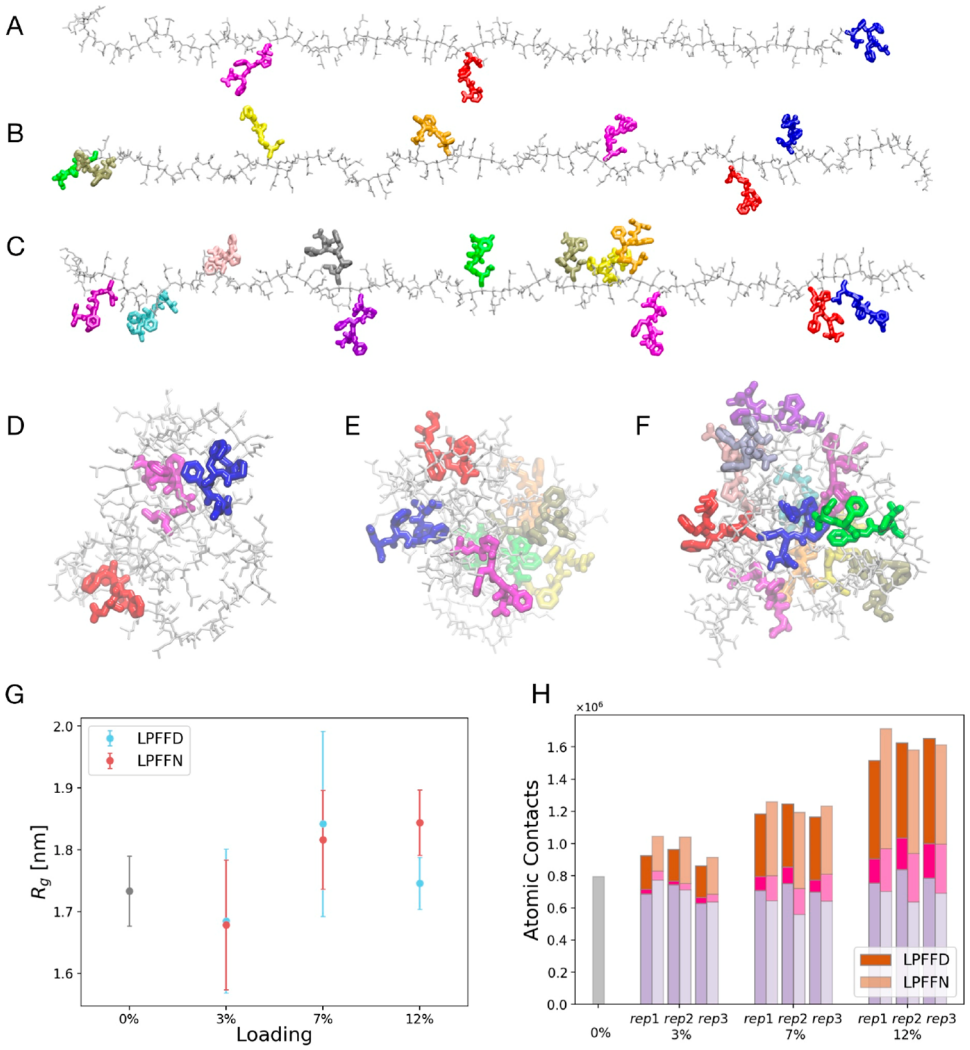

Figure 4. MD simulations illustrate the importance of ligand−ligand contacts in mPPC globular structures. Three replicas of mPPC models (DP = 100) were generated with 3, 7, and 12 copies of LD and LN. The extended (A−C) and equilibrated (D−F) structures containing 3 (A,D), 7 (B,E), and 12 (C,F) copies of LD before and after simulation. The polymer backbone is shown in gray; LD ligands are shown in varied colors. (G) Radius of gyration (R_g) of the equilibrated mPPC models (averaged over three replicas in each case). (H) Atomic contacts (3.5 Å cutoff) extracted for polymer−polymer (violet), peptide−peptide (magenta), and polymer−peptide (brown) interactions in globular mPPC structures.

(the ratio between the lag time of the control and that in the presence of mPPCs) against concentration (Figure 3B). We defined a critical concentration ($c_{1/3}$) at which the mPPC extends the lag time to 300% of the control and used it to evaluate mPPC potency. The extension (300%) was arbitrarily chosen for the best differentiation of mPPC potency due to the lack of appropriate models for mPPC−Aβ binding. The determined $c_{1/3}$ values of all mPPCs are represented graphically in Figure 3C and they fall in the 10−150 μg/mL range.

We noticed that the critical concentration for 7 out of 27 mPPCs was equal to or lower than the Aβ_{40} concentration (43 μg/mL), which highlights a remarkable inhibitory potency for these mPPCs. While no set of parameters or trends consistently resulted in optimal mPPCs (lowest $c_{1/3}$) for all three ligands, we did gain insight into the interplay of ligand loading and polymer MW for each ligand. For the negatively charged ligand LD, a loading percentage close to 7% consistently led to the maximum inhibition for all MWs. The same phenomenon was not observed for neutral ligands LN or GA. Other than the two abnormally sized LN-mPPCs, we found that an optimized number of copies in LN-mPPCs, that is, higher loading for low MW and lower loading for higher MW, leads to better inhibition. Since LD and LN only differ by the amidation of one side chain, differences of ligand loading dependence must result from the charge of the ligand. Our hypothesis is supported by a similar trend for another neutral ligand, GA. We also found that, to achieve similar levels of inhibition for LN-mPPCs, a higher ligand loading is necessary for GA-mPPCs. This is tentatively ascribed to a lower hydrogen bond donor capacity for methylated ligand GA. As for the effects of MW on inhibition, mPPCs obtained from higher MW precursors are generally less potent. This is not surprising considering that at the same mass concentration, a higher MW translates into a lower mPPC-to-Aβ molar ratio. Because of the compositional differences of mPPCs, we primarily use mass concentration in the discussion (Figure S3). We also analyzed the results in terms of molar concentration of the peptide ligand and found similar trends (Figure S3). LD-mPPCs still perform the best at 7% loading, whereas for the neutral ligands the lower loading mPPCs generally outperform the higher loading ones.

DOI: 10.1021/acsmacrolett.9b00559
ACS Macro Lett. 2019, 8, 1365−1371

Examining the accessible conformational space of mPPCs is a critical step toward the understanding of the mPPC inhibition mechanism and its MW or loading dependencies. To that end, we performed extensive all-atom MD simulations on model mPPCs containing LD or LN ligands at different loadings (3, 7, and 12%) and polymer MWs (DP of 100, 300, and 500; equivalent to polymer precursors of 16−78 kDa MW). Three replicas were generated for DP 100 (analogous to the 18 kDa polymer) models of 3, 7, and 12% ligand loading, and all of them quickly formed a globular structure within the first 20 ns of the simulation. It was found that the structural heterogeneity from a random grafting pattern of ligands has a limited effect on equilibrated structures of DP 100 models (Table S4). As a result, only one model for each composition was generated for DP 300 and DP 500 mPPCs, whose reorganization into stable globular structures took over 100 ns (Figure S4). While it is possible that the obtained equilibrated structures may not be the most thermodynamically stable, structural analyses were nonetheless performed as they represent local minima in the potential energy surface. As a measure of the mPPC size, radius of gyration (R_g) was calculated for structures from the last 50 ns of each trajectory and reported in Figures 4G and S4. For the mPPC models at low MW (DP = 100), R_g increased only when the loading raised from 3 to 7%, but decreased or stayed about the same when the loading increased from 0 to 3% or from 7 to 12% (Figure 4G). It is known that the hydrodynamic radius obtained from DLS is larger than the radius of gyration for simulated globular particles, and implicit solvent used in our simulations may result in underestimated particle sizes.[32] DP 300 and DP 500 models showed an evident contraction of LN-mPPCs (Figure S6). Such contraction was absent for LD-mPPCs at the same MW, which might be related to limited simulation time, as larger-scale structural rearrangements may not be captured within the simulation time frame. Nevertheless, the formation of globular structures for mPPCs is consistently observed in all simulations.

Further interaction analyses revealed that the mPPC globular structures are promoted by hydrophobic interactions as well as hydrogen bonds (Figures 4H and S5). The contraction in mPPC size is associated with an increase in intramolecular interactions between the ligands. At higher loadings, interaction between the hydrophobic peptide residues becomes a dominant factor; as a result, the ligands pack more tightly inside the core of mPPCs. The hydrophilic PHPMA polymer backbone (rich in hydroxyl groups), on the other hand, tends to position itself on the periphery of the globular structure to maximize interaction with the aqueous phase. This effect was more pronounced for LN-mPPCs, where the absence of a net charge in the ligand leads to stronger ligand−ligand interactions and eventually a higher level of polymer contraction. Data supporting these conclusions are provided in plots of R_g (Figure S6), which is systematically smaller for LN-mPPCs. Since the contraction of mPPCs at high loadings translates into decreased ligand accessibility, these simulation results provide an explanation for the experimentally observed dependence of LD- and LN-mPPCs efficacy on peptide loading level. The significant role of hydrophobic interactions in mPPC folding also explains why a higher loading is needed for the neutral, less hydrophobic ligand GA than LN.

In conclusion, we have shown that mPPCs represent a general strategy to access Aβ inhibitors with enhanced potency. We established that the ligand scope is limited to peptides/peptoids that are similar to but not directly derived from the native Aβ sequence. LD-mPPCs with a negatively charged LPFFD ligand were more efficient inhibitors and were most effective at 7% loading. In contrast, the optimal loading varies for conjugates of the neutral ligands of different MWs. Collectively, the experimental and simulation results reveal the key yet subtle role of hydrophobic ligand−ligand interactions in mPPC behavior. While they are instrumental to the formation of globular mPPC structures and the increased local concentration of active ligands, an excess of ligand−ligand interactions leads to contracted structures where ligands are unavailable for interactions with Aβ. Thus, achieving optimal inhibition requires a delicate balance between ligand−ligand and ligand−Aβ interactions. The ligand LD, which contains a negatively charged Asp residue, illustrates this balance as it outperforms the two neutral ligands. Our results illustrate the opportunities for inhibitor development in the mPPC chemical space, for example, by employing more potent peptides/peptidomimetics as ligands and by including additional functional groups for targeted delivery. Our findings also pave the way for the use of mPPCs as a general platform to target protein aggregation in a variety of other deposition diseases in addition to AD.

■ ASSOCIATED CONTENT

Supporting Information

The Supporting Information is available free of charge on the ACS Publications website at DOI: 10.1021/acsmacrolett.9b00559.

The synthesis and characterization of mPPCs, experimental details of the ThT assay, and methods and additional results of MD simulations (PDF).

■ AUTHOR INFORMATION

Corresponding Authors

*E-mail: qchen20@illinois.edu(Q.C).
*E-mail: emad@life.illinois.edu(E.T.).
*E-mail: rienstra@illinois.edu(C.M.R.).
*E-mail: jsmoore@illinois.edu(J.S.M.).

ORCID

Xing Jiang: 0000-0001-8259-1948
Yang Song: 0000-0002-9279-3284
Qian Chen: 0000-0002-1968-441X
Emad Tajkhorshid: 0000-0001-8434-1010
Chad M. Rienstra: 0000-0002-9912-5596
Jeffrey S. Moore: 0000-0001-5841-6269

Author Contributions

†These authors contributed equally to this work.

Notes

The authors declare no competing financial interest.

■ ACKNOWLEDGMENTS

This research is supported by funding from the Arnold and Mabel Beckman Foundation (Beckman Institute Postdoctoral Fellowship, University of Illinois, Urbana−Champaign, X.J.), the U.S. Air Force Office of Scientific Research Young Investigator Program (AFOSR-YIP, FA9550-17-1-0296, Q.C.) and Defense University Research Instrumentation Program (FA9550-18-1-0393, Q.C.), National Institutes of Health (P41-GM104601, R01-GM123455, and R01-

DOI: 10.1021/acsmacrolett.9b00559
ACS Macro Lett. 2019, 8, 1365−1371

GM067887, E.T.; R01-GM123455, C.M.R.), and the U.S. Department of Energy, Office of Basic Energy Sciences, Division of Materials Sciences and Engineering (Award No. DE-FG02-07ER46471, J.S.M). Simulations were performed using National Science Foundation computing resources allocated through an XSEDE grant (MCA06N060, E.T.) and Illinois Blue Waters allocation (to E.T.) at the National Center for Supercomputing Applications at the University of Illinois. We thank Shijia Tang and Liuyan Tang for their assistance and discussions and Prof. Cathy Murphy for access to the DLS instrument.

REFERENCES

(1) Glenner, G. G.; Wong, C. W. Alzheimer's Disease: Initial Report of the Purification and Characterization of a Novel Cerebrovascular Amyloid Protein. *Biochem. Biophys. Res. Commun.* **1984**, *120*, 885−890.

(2) Han, X.; He, G. Toward a Rational Design to Regulate β-Amyloid Fibrillation for Alzheimer's Disease Treatment. *ACS Chem. Neurosci.* **2018**, *9*, 198−210.

(3) Goyal, D.; Shuaib, S.; Mann, S.; Goyal, B. Rationally Designed Peptides and Peptidomimetics as Inhibitors of Amyloid-β (Aβ) Aggregation: Potential Therapeutics of Alzheimer's Disease. *ACS Comb. Sci.* **2017**, *19*, 55−80.

(4) Sun, H.; Liu, J.; Li, S.; Zhou, L.; Wang, J.; Liu, L.; Lv, F.; Gu, Q.; Hu, B.; Ma, Y.; Wang, S. Reactive Amphiphilic Conjugated Polymers for Inhibiting Amyloid β Assembly. *Angew. Chem., Int. Ed.* **2019**, *58*, 5988−5993.

(5) Cabaleiro-Lago, C.; Quinlan-Pluck, F.; Lynch, I.; Lindman, S.; Minogue, A. M.; Thulin, E.; Walsh, D. M.; Dawson, K. A.; Linse, S. Inhibition of Amyloid β Protein Fibrillation by Polymeric Nanoparticles. *J. Am. Chem. Soc.* **2008**, *130*, 15437−15443.

(6) Fasting, C.; Schalley, C. A.; Weber, M.; Seitz, O.; Hecht, S.; Koksch, B.; Dernedde, J.; Graf, C.; Knapp, E. W.; Haag, R. Multivalency as a Chemical Organization and Action Principle. *Angew. Chem., Int. Ed.* **2012**, *51*, 10472−10498.

(7) Gestwicki, J. E.; Cairo, C. W.; Strong, L. E.; Oetjen, K. A.; Kiessling, L. L. Influencing Receptor−Ligand Binding Mechanisms with Multivalent Ligand Architecture. *J. Am. Chem. Soc.* **2002**, *124*, 14922−14933.

(8) Soto, C.; Sigurdsson, E. M.; Morelli, L.; Kumar, R. A.; Castaño, E. M.; Frangione, B. β-Sheet Breaker Peptides Inhibit Fibrillogenesis in a Rat Brain Model of Amyloidosis: Implications for Alzheimer's Therapy. *Nat. Med.* **1998**, *4*, 822−826.

(9) Soto, C.; Kindy, M. S.; Baumann, M.; Frangione, B. Inhibition of Alzheimer's Amyloidosis by Peptides That Prevent β -Sheet Conformation. *Biochem. Biophys. Res. Commun.* **1996**, *226*, 672−680.

(10) Song, Y.; Cheng, P.-N.; Zhu, L.; Moore, E. G.; Moore, J. S. Multivalent Macromolecules Redirect Nucleation-Dependent Fibrillar Assembly into Discrete Nanostructures. *J. Am. Chem. Soc.* **2014**, *136*, 5233−5236.

(11) Smith, J. W.; Jiang, X.; An, H.; Barclay, A. M.; Licari, G.; Tajkhorshid, E.; Moore, E. G.; Rienstra, C. M.; Moore, J. S.; Chen, Q. Polymer−Peptide Conjugates Convert Amyloid into Protein Nanobundles through Fragmentation and Lateral Association. *ACS Appl. Nano Mater.* **2019**, na DOI: 10.1021/acsanm.9b01331.

(12) Song, Y.; Moore, E. G.; Guo, Y.; Moore, J. S. Polymer − Peptide Conjugates Disassemble Amyloid β Fibrils in a Molecular-Weight Dependent Manner. *J. Am. Chem. Soc.* **2017**, *139*, 4298−4301.

(13) Song, Y. PhD Thesis. School of Chemical Sciences, University of Illinois, Urbana-Champaign, 2017.

(14) Minicozzi, V.; Chiaraluce, R.; Consalvi, V.; Giordano, C.; Narcisi, C.; Punzi, P.; Rossi, G. C.; Morante, S. Computational and Experimental Studies on β-Sheet Breakers Targeting $A\beta_{1-40}$ Fibrils. *J. Biol. Chem.* **2014**, *289*, 11242−11252.

(15) Tjernberg, L. O.; Näslund, J.; Lindqvist, F.; Johansson, J.; Karlström, A. R.; Thyberg, J.; Terenius, L.; Nordstedt, C. Arrest of β-Amyloid Fibril Formation by a Pentapeptide Ligand. *J. Biol. Chem.* **1996**, *271*, 8545−8548.

(16) Rajasekhar, K.; Suresh, S. N.; Manjithaya, R.; Govindaraju, T. Rationally Designed Peptidomimetic Modulators of Aβ Toxicity in Alzheimer's Disease. *Sci. Rep.* **2015**, *5*, 8139.

(17) Moraes, J.; Simionca, I. M.; Ketari, H.; Klok, H. A. Avoiding Compositional Drift during the RAFT Copolymerization of *N*-(2-hydroxypropyl)-methacrylamide and *N*-acryloxysuccinimide: Towards Uniform Platforms for Post-polymerization Modification. *Polym. Chem.* **2015**, *6*, 3245−3251.

(18) Yanjarappa, M. J.; Gujraty, K. V.; Joshi, A.; Saraph, A.; Kane, R. S. Synthesis of Copolymers Containing an Active Ester of Methacrylic Acid by RAFT: Controlled Molecular Weight Scaffolds for Biofunctionalization. *Biomacromolecules* **2006**, *7*, 1665−1670.

(19) In our previous reports (refs 12 and 13), the MW of polymer precursors to the mPPCs was determined by size exclusion chromatography with polystyrene standards and deviates significantly from the ones determined by multi-angle light scattering.

(20) Goldsbury, C. S.; Wirtz, S.; Müller, S. A.; Sunderji, S.; Wicki, P.; Aebi, U.; Frey, P. Studies on the *in Vitro* Assembly of Aβ 1−40: Implications for the Search for Aβ Fibril Formation Inhibitors. *J. Struct. Biol.* **2000**, *130*, 217−231.

(21) Jarrett, J. T.; Lansbury, P. T. Seeding "One-Dimensional Crystallization" of Amyloid: a Pathogenic Mechanism in Alzheimer's Disease and Scrapie? *Cell* **1993**, *73*, 1055−1058.

(22) Arosio, P.; Vendruscolo, M.; Dobson, C. M.; Knowles, T. P. J. Chemical Kinetics for Drug Discovery to Combat Protein Aggregation Diseases. *Trends Pharmacol. Sci.* **2014**, *35*, 127−135.

(23) Li, M.; Howson, S. E.; Dong, K.; Gao, N.; Ren, J.; Scott, P.; Qu, X. Chiral Metallohelical Complexes Enantioselectively Target Amyloid β for Treating Alzheimer's Disease. *J. Am. Chem. Soc.* **2014**, *136*, 11655−11663.

(24) Cheng, P.-N.; Liu, C.; Zhao, M.; Eisenberg, D.; Nowick, J. S. Amyloid β-Sheet Mimics that Antagonize Amyloid Aggregation and Reduce Amyloid Toxicity. *Nat. Chem.* **2012**, *4*, 927−933.

(25) Wallin, C.; Hiruma, Y.; Wärmländer, S. K. T. S.; Huvent, I.; Jarvet, J.; Abrahams, J. P.; Gräslund, A.; Lippens, G.; Luo, J. The Neuronal Tau Protein Blocks *in Vitro* Fibrillation of the Amyloid-β (Aβ) Peptide at the Oligomeric Stage. *J. Am. Chem. Soc.* **2018**, *140*, 8138−8146.

(26) Xu, Z.; Jia, S.; Wang, W.; Yuan, Z.; Ravoo, B. J.; Guo, D.-S. Heteromultivalent Peptide Recognition by Co-Assembly of Cyclodextrin and Calixarene Amphiphiles Enables Inhibition of Amyloid Fibrillation. *Nat. Chem.* **2019**, *11*, 86−93.

(27) Gao, N.; Sun, H.; Dong, K.; Ren, J.; Qu, X. Gold-Nanoparticle-Based Multifunctional Amyloid-β Inhibitor Against Alzheimer's Disease. *Chem. - Eur. J.* **2015**, *21*, 829−835.

(28) Le Droumaguet, B.; Nicolas, J.; Brambilla, D.; Mura, S.; Maksimenko, A.; De Kimpe, L.; Salvati, E.; Zona, C.; Airoldi, C.; Canovi, M.; Gobbi, M.; Magali, N.; La Ferla, B.; Nicotra, F.; Scheper, W.; Flores, O.; Masserini, M.; Andrieux, K.; Couvreur, P. Versatile and Efficient Targeting Using a Single Nanoparticulate Platform: Application to Cancer and Alzheimer's Disease. *ACS Nano* **2012**, *6*, 5866−5879.

(29) Reinke, A. A.; Ung, P. M. U.; Quintero, J. J.; Carlson, H. A.; Gestwicki, J. E. Chemical Probes That Selectively Recognize the Earliest Aβ Oligomers in Complex Mixtures. *J. Am. Chem. Soc.* **2010**, *132*, 17655−17657.

(30) Chafekar, S. M.; Malda, H.; Merkx, M.; Meijer, E. W.; Viertl, D.; Lashuel, H. A.; Baas, F.; Scheper, W. Branched KLVFF Tetramers Strongly Potentiate Inhibition of β-Amyloid Aggregation. *ChemBioChem* **2007**, *8*, 1857−1864.

(31) Watanabe, K.-I.; Nakamura, K.; Akikusa, S.; Okada, T.; Kodaka, M.; Konakahara, T.; Okuno, H. Inhibitors of Fibril Formation and Cytotoxicity of β-Amyloid Peptide Composed of KLVFF Recognition Element and Flexible Hydrophilic Disrupting Element. *Biochem. Biophys. Res. Commun.* **2002**, *290*, 121−124.

(32) (a) Mizuta, K.; Ishii, Y.; Kim, K.; Matubayasi, N. Bridging the Gap between Molecular Dynamics and Hydrodynamics in Nanoscale

DOI: 10.1021/acsmacrolett.9b00559
ACS Macro Lett. 2019, 8, 1365−1371

Brownian Motions. *Soft Matter* **2019**, *15*, 4380−4390. (b) Lazzari, F.; Manfredi, A.; Alongi, J.; Mendichi, R.; Ganazzoli, F.; Raffaini, G.; Ferruti, P.; Ranucci, E. Self-Structuring in Water of Polyamidoamino Acids with Hydrophobic Side Chains Deriving from Natural α-Amino Acids. *Polymers* **2018**, *10*, 1261.

DOI: 10.1021/acsmacrolett.9b00559
ACS Macro Lett. 2019, 8, 1365−1371